

Combined first-principles calculations of electron-electron and electron-phonon self-energies in condensed systems

Han Yang,^{†,‡} Marco Govoni,^{*,¶,‡} Arpan Kundu,[‡] and Giulia Galli^{*,†,‡,¶}

[†]*Department of Chemistry, University of Chicago, Chicago, Illinois 60637, United States*

[‡]*Pritzker School of Molecular Engineering, The University of Chicago, Chicago, Illinois 60637, United States*

[¶]*Materials Science Division and Center for Molecular Engineering, Argonne National Laboratory, Lemont, Illinois 60439, United States*

E-mail: mgovoni@anl.gov; gagalli@uchicago.edu

Abstract

We present a method to efficiently combine the computation of electron-electron and electron-phonon self-energies, which enables the evaluation of electron-phonon coupling at the G_0W_0 level of theory for systems with hundreds of atoms. In addition, our approach, which is a generalization of a method recently proposed for molecules [*J. Chem. Theory Comput.* 2018, **14**, 6269–6275], enables the inclusion of non-adiabatic and temperature effects at no additional computational cost. We present results for diamond and defects in diamond and discuss the importance of numerically accurate G_0W_0 band structures to obtain robust predictions of zero point renormalization (ZPR) of band gaps, and of the inclusion of non-adiabatic effect to accurately compute the ZPR of defect states in the band gap.

Introduction

The interaction between electrons and phonons in solids¹⁻³ gives rise to a variety of interesting physical phenomena, including superconductivity,⁴ and to complex electronic structure properties in metals, semiconductors and insulators.⁵ Electron-phonon coupling has been widely studied for more than half a century.⁶ However, it is only in the last two decades that first principles, quantum mechanical methods have been applied to carry out quantitative calculations,^{1,3,7} based on frozen-phonon approaches,^{3,8} density functional perturbation theory (DFPT)^{1,3,9-13} and, very recently, path-integral molecular dynamics simulations based on density functional theory (DFT).¹⁴

Most calculations of electron-phonon coupling in solids solve the electronic structure problem at the level of density functional theory (DFT),^{3,12,13} although it has been shown that for several solids many body perturbation theory (MBPT)^{2,3,15} is necessary, in order to obtain results in quantitative agreement with experiments. Given the computational cost involved in electron-phonon calculations based on MBPT, e.g., at the G_0W_0 level, plasmon-pole models (PPM) are often employed^{3,15} to approximate the frequency dependence of the self-energy, in spite of some known deficiencies of such models.¹⁶

With the goal of improving the accuracy and efficiency of electron-phonon calculations within MBPT, we recently proposed¹⁷ a method that combines the evaluation of electron-electron and electron-phonon self-energies. The dielectric matrix is represented in terms of dielectric eigenpotentials,¹⁸ utilized for both the calculation of G_0W_0 quasi-particle energies and the diagonalization of the dynamical matrix; virtual electronic states are not explicitly computed, dielectric matrices, being represented using a spectral decomposition, are never inverted, and all self-energies are evaluated over the full frequency spectrum using the Lanczos algorithm.¹⁹⁻²¹ Importantly, our implementation also enables at no extra cost the evaluation of non-adiabatic effects and electron-phonon self energies at multiple temperatures and frequencies. Although in principle the method is general, in practice it has so far been applied only to finite systems within the adiabatic approximation.

In this work, we generalize the combined electron-electron and electron-phonon approach described in Ref. 17 to solids and, after presenting a detailed verification and validation protocol, we apply the approach to large supercells with about 1000 electrons, which are representative of defective solids. We report results as a function of temperature and we study in detail the effect of including non-adiabatic terms in the zero point renormalization of the band gap of pristine and defective diamond and on defect states.

The rest of this work is organized as follows: we first describe our methodology and then verify our implementation and validate our results for specific systems; we then present applications of the method to point defects in diamond.

Methodology

Dynamical and electron-phonon coupling matrices

In a periodic system, phonon frequencies are computed by diagonalizing the dynamical matrix¹⁰

$$D_{I\alpha,J\beta}(\mathbf{q}) = \frac{1}{\sqrt{M_I M_J}} C_{I\alpha,J\beta}(\mathbf{q}) = \frac{1}{\sqrt{M_I M_J}} \frac{\partial^2 E}{\partial u_{I\alpha}^*(\mathbf{q}) \partial u_{J\beta}(\mathbf{q})} \quad (1)$$

where $C_{I\alpha,J\beta}(\mathbf{q})$ is a force constant, E is the total energy of the system, u denotes displacements from equilibrium atomic positions, M_I , M_J are atomic masses, I , J are indices of atoms, α , β are Cartesian directions, and \mathbf{q} is the wave-vector of the phonon mode.

The force constants are given by the sum of an electronic and ionic part, with the latter being trivial to evaluate. Within the framework of density functional perturbation theory (DFPT), the electronic contribution can be written as

$$C_{I\alpha,J\beta}^{elec}(\mathbf{q}) = \sum_n \sum_{\mathbf{k}}^{occ} w_{\mathbf{k}} \langle \psi_{n\mathbf{k}} | \partial_{J\beta,\mathbf{q}} V_{ext} | \partial_{I\alpha,\mathbf{q}} \psi_{n\mathbf{k}} \rangle + c.c., \quad (2)$$

where \mathbf{k} is a k-point within the Brillouin zone with weight $w_{\mathbf{k}}$, $\psi_{n\mathbf{k}}$ is the wavefunction of the n -th band at \mathbf{k} , and V_{ext} is the external ionic potential. For simplicity, we denoted the

derivative $\partial/\partial u_{I\alpha}(\mathbf{q})$ as $\partial_{I\alpha,\mathbf{q}}$. The bracket in Eq. 2 is commonly computed by solving the Sternheimer equation self-consistently,

$$(\hat{H}_{KS} - \varepsilon_{n\mathbf{k}}) |\partial_{I\alpha,\mathbf{q}} \psi_{n\mathbf{k}}\rangle = -\hat{\mathcal{P}}_{\mathbf{k}+\mathbf{q}}^c \partial_{I\alpha,\mathbf{q}} \hat{V}_{SCF} |\psi_{n\mathbf{k}}\rangle, \quad (3)$$

where $\hat{H}_{KS} = \hat{K} + \hat{V}_{SCF}$ is the Kohn-Sham Hamiltonian; \hat{K} is the kinetic operator; \hat{V}_{SCF} is the self-consistent potential operator; $\varepsilon_{n\mathbf{k}}$ is the Kohn-Sham eigenvalue of the n -th band at the \mathbf{k} point, $\partial_{I\alpha,\mathbf{q}} \hat{V}_{SCF}$ is the first order change of the self-consistent potential due to atomic displacements, $\partial_{I\alpha,\mathbf{q}} \psi_{n\mathbf{k}}$ denotes the first order change of the wavefunction, and $\hat{\mathcal{P}}_{\mathbf{k}+\mathbf{q}}^c = \hat{I} - \sum_v^{occ} |\psi_{v\mathbf{k}+\mathbf{q}}\rangle \langle \psi_{v\mathbf{k}+\mathbf{q}}|$ is the projection operator onto the manifold of unoccupied (virtual) single particle electronic states.

Instead of solving the Sternheimer equation self-consistently, we write the bracket in Eq. 2 as:¹⁷

$$\langle \psi_{n\mathbf{k}} | \partial_{J\beta,\mathbf{q}} V_{ext} | \partial_{I\alpha,\mathbf{q}} \psi_{n\mathbf{k}} \rangle = \langle \partial_{J\beta,\mathbf{q}} \psi_{n\mathbf{k}}^{bare} | \partial_{I\alpha,\mathbf{q}} V_{SCF} | \psi_{n\mathbf{k}} \rangle, \quad (4)$$

where the change of the wavefunction is obtained through the one-shot solution of the Sternheimer equation

$$(\hat{H}_{KS} - \varepsilon_{n\mathbf{k}}) |\partial_{I\alpha,\mathbf{q}} \psi_{n\mathbf{k}}^{bare}\rangle = -\hat{\mathcal{P}}_{\mathbf{k}+\mathbf{q}}^c \partial_{I\alpha,\mathbf{q}} \hat{V}_{ext} |\psi_{n\mathbf{k}}\rangle. \quad (5)$$

The change of SCF potential can be evaluated from $\partial_{I\alpha,\mathbf{q}} \hat{V}_{ext}$ as

$$\partial_{I\alpha,\mathbf{q}} V_{SCF} = \partial_{I\alpha,\mathbf{q}} V_{ext} + [f_{Hxc} + f_{Hxc} \chi f_{Hxc}] \partial_{I\alpha,\mathbf{q}} \rho^{bare} \quad (6)$$

where $f_{Hxc} = v_c + f_{xc}$ is the sum of the bare Coulomb potential, v_c , and the exchange-correlation kernel, f_{xc} ; χ is the reducible density-density response function and $\partial_{I\alpha,\mathbf{q}} \rho^{bare}$ is the derivative of the bare change of density,

$$\partial_{I\alpha,\mathbf{q}} \rho^{bare} = \sum_n^{occ} \sum_{\mathbf{k}} w_{\mathbf{k}} [\psi_{n\mathbf{k}}^* \partial_{I\alpha,\mathbf{q}} \psi_{n\mathbf{k}}^{bare} + c.c.] \quad (7)$$

In order to efficiently evaluate the reducible density-density response function, χ , we represent the irreducible density-density response function, χ_0 , in terms of projective dielectric eigenpotentials (PDEP)^{18–20} and we represent χ with the same basis used as that of χ_0 :

$$\chi_0(\mathbf{q}) = \sum_i^{N_{\text{PDEP}}} |\phi_i(\mathbf{q})\rangle \lambda_i(\mathbf{q}) \langle \phi_i(\mathbf{q})|, \quad (8)$$

where i is the index of the PDEP basis, $\phi_i(\mathbf{q})$ and $\lambda_i(\mathbf{q})$ are the i -th eigenvector and eigenvalue of the symmetrized reducible polarizability, N_{PDEP} is the number of PDEP basis functions, respectively. Using the Dyson equation $\chi = \chi_0 + \chi_0 f_{Hxc} \chi$, the reducible density-density response function can be evaluated using the PDEP basis set:

$$\chi = (1 - \chi_0 f_{Hxc})^{-1} \chi_0. \quad (9)$$

Adopting the procedure described above, we can compute the dynamical matrix $D(\mathbf{q})$:

$$\sum_{J\beta} D_{I\alpha, J\beta}(\mathbf{q}) \xi_{J\beta, \mathbf{q}\nu} = \omega_{\mathbf{q}\nu}^2 \xi_{I\alpha, \mathbf{q}\nu}, \quad (10)$$

where $\omega_{\mathbf{q}\nu}$ are phonon frequencies and $\xi_{I\alpha, \mathbf{q}\nu}$ are phonon eigenvectors. Finally, Eq. 6 is used to evaluate the electron-phonon coupling matrix elements g given by:¹

$$g_{mn\nu}(\mathbf{k}, \mathbf{q}) = \langle \psi_{m\mathbf{k}+\mathbf{q}} | \partial_{\mathbf{q}\nu} V_{SCF} | \psi_{n\mathbf{k}} \rangle, \quad (11)$$

where $\partial_{\mathbf{q}\nu} V_{SCF}$ is the mode-resolved change of potential,

$$\partial_{\mathbf{q}\nu} V_{SCF} = \sum_{I\alpha} \frac{\xi_{I\alpha, \mathbf{q}\nu}}{\sqrt{2M_I \omega_{\mathbf{q}\nu}}} \partial_{I\alpha, \mathbf{q}} V_{SCF} \quad (12)$$

Electron-phonon self-energy

Within many-body perturbation theory (MBPT),^{1,16} the electron-phonon self-energy has two components, the Fan-Migdal:

$$\Sigma_{n\mathbf{k}}^{\text{FM}}(\omega, T) = \sum_{m\nu\mathbf{q}} |g_{mn\nu}(\mathbf{k}, \mathbf{q})|^2 \left[\frac{n_{\mathbf{q}\nu} + f_{m\mathbf{k}+\mathbf{q}}}{\omega - \varepsilon_{m\mathbf{k}+\mathbf{q}} + \omega_{\mathbf{q}\nu} - i0^+} + \frac{n_{\mathbf{q}\nu} + 1 - f_{m\mathbf{k}+\mathbf{q}}}{\omega - \varepsilon_{m\mathbf{k}+\mathbf{q}} - \omega_{\mathbf{q}\nu} - i0^+} \right] \quad (13)$$

and Debye-Waller:

$$\Sigma_{n\mathbf{k}}^{\text{DW}}(T) = - \sum_{m\nu\mathbf{q}} \sum_{I\alpha J\beta} \frac{2n_{\mathbf{q}\nu} + 1}{\varepsilon_{n\mathbf{k}} - \varepsilon_{m\mathbf{k}}} \frac{1}{4\omega_{\mathbf{q}\nu}} \left[\frac{\xi_{I\alpha, \mathbf{q}\nu} \xi_{I\beta, \mathbf{q}\nu}^*}{M_I} + \frac{\xi_{J\alpha, \mathbf{q}\nu} \xi_{J\beta, \mathbf{q}\nu}^*}{M_J} \right] g_{mn}^{*, I\alpha}(\mathbf{k}, \mathbf{0}) g_{mn}^{J\beta}(\mathbf{k}, \mathbf{0}), \quad (14)$$

where $n_{\mathbf{q}\nu}$ and $f_{m\mathbf{k}+\mathbf{q}}$ are Bose-Einstein and Fermi-Dirac distributions, respectively. Most electron-phonon calculations reported in the literature use the Allen-Heine-Cardona (AHC) formalism,^{22,23} and hence two main approximations: the on-mass-shell approximation, i.e., $\omega = \varepsilon_{n\mathbf{k}}$, and the adiabatic approximation, i.e., $\varepsilon_{n\mathbf{k}} - \varepsilon_{m\mathbf{k}+\mathbf{q}} \gg \omega_{\mathbf{q}\nu}$. Within these approximations, the real part of the Fan-Migdal self-energy can be simplified:

$$\text{Re } \Sigma_{n\mathbf{k}}^{\text{FM}}(T) \approx \sum_{m\nu\mathbf{q}} |g_{mn\nu}(\mathbf{k}, \mathbf{q})|^2 \left[\frac{2n_{\mathbf{q}\nu} + 1}{\varepsilon_{n\mathbf{k}} - \varepsilon_{m\mathbf{k}+\mathbf{q}}} \right]. \quad (15)$$

To avoid summations over empty bands in the evaluation of Fan-Migdal and Debye-Waller self-energies (Eq. 13-15), here we use the Lanczos approach. Writing the Fan-Migdal self-energy within the AHC approximation (Eq. 15) as an example, we first expand the electron-phonon coupling matrix using Eq. 11,

$$\Sigma_{n\mathbf{k}}^{\text{FM}} = \sum_{m\nu\mathbf{q}} \langle \psi_{n\mathbf{k}} | \partial_{-\mathbf{q}\nu} V_{SCF} | \psi_{m\mathbf{k}+\mathbf{q}} \rangle \frac{2n_{\mathbf{q}\nu} + 1}{\varepsilon_{n\mathbf{k}} - \varepsilon_{m\mathbf{k}+\mathbf{q}}} \langle \psi_{m\mathbf{k}+\mathbf{q}} | \partial_{\mathbf{q}\nu} V_{SCF} | \psi_{n\mathbf{k}} \rangle. \quad (16)$$

Given the projection of the Hamiltonian on the conduction (virtual) manifold, i.e., $\tilde{H}_{\mathbf{k}+\mathbf{q}} =$

$\hat{\mathcal{P}}_{\mathbf{k}+\mathbf{q}}^c H \hat{\mathcal{P}}_{\mathbf{k}+\mathbf{q}}^c$, we can write

$$\sum_m |\psi_{m\mathbf{k}+\mathbf{q}}\rangle (\varepsilon_{n\mathbf{k}} - \varepsilon_{m\mathbf{k}+\mathbf{q}})^{-1} \langle \psi_{m\mathbf{k}+\mathbf{q}}| = (\varepsilon_{n\mathbf{k}} - \tilde{H}_{\mathbf{k}+\mathbf{q}})^{-1}. \quad (17)$$

Eq. 17 may be efficiently solved using the Lanczos approach (a detailed derivation is presented in the SI), and the imaginary part of the Fan-Midgal self energy and the Debye-Waller self-energy (Eq. 13-14) may be computed in a similar manner.

The approach described above was implemented in the `WEST` code,^{17,20} interfaced with `Quantum Espresso` (version 6.1)²⁴ and the symmetries at \mathbf{k} and \mathbf{q} points were analyzed using the `PHonon` package.²⁴

A brief summary of the main features of the methodology presented here, compared to the implementations of first principles electron-phonon calculations used in the current literature, is given in Table 1.

Table 1: First principles calculations of electron-phonon self-energies based on the G_0W_0 approximation. The integral of the self energy as a function of frequency is evaluated using either a plasmon-pole model (PPM) or by carrying out full-frequency (FF) integration using contour deformation.^{20,25} Evaluation of the G_0W_0 self-energy ($\Sigma_{G_0W_0}$) and of the electron-phonon self-energy (Σ_{ep}) are performed with algorithms requiring summation (S) over virtual states or no summation (NS) over virtual states. The evaluation of $\Sigma_{G_0W_0}$ and Σ_{ep} is combined in this work (Y) but carried out separately (N) in previous works.

	Ref. 2	Ref. 3	This work
Frequency Integration	PPM	PPM	FF
Evaluation of $\Sigma_{G_0W_0}$	S ^a	S	NS
Evaluation of Σ_{ep}	S	S/NS ^b	NS
Combined evaluation of $\Sigma_{G_0W_0}$ and Σ_{ep}	N	N	Y

^a The G_0W_0 energy levels were not used in the evaluation of electron-phonon self-energies at G_0W_0 level, instead a scissor operator corresponding to the G_0W_0 correction was applied to DFT energy levels.

^b No empty bands were used in the evaluation of electron-phonon self-energies at the DFT level. No information was provided on the calculations of empty states for G_0W_0 calculations.

Verification protocol

Our verification protocol includes first the comparison of phonon frequencies computed with standard DFPT based approaches with those of our methodology (Eq. 6); we then carry out a study of the numerical parameters affecting the calculations of the ZPR of diamond within DFT and G_0W_0 and compare our results with those present in the literature.

Phonon frequencies – To verify our implementation, we first compared the phonon frequencies of the diamond crystal obtained with the method described above to those computed with the PHonon package in Quantum Espresso.²⁴ For verification purposes we carried out our calculations using the local density approximation (LDA), a cutoff of 60 Ry, Trouiller-Martins type pseudopotentials²⁶ generated with the FHI98pp code,²⁷ and a $3 \times 3 \times 3$ \mathbf{k} -point mesh. Fig. S1 shows that the interpolated phonon dispersion curves in diamond obtained with the two approaches are indistinguishable, with a mean absolute difference less than 1 cm^{-1} . The comparison was repeated using energy cutoffs of 80, 100, and 120 Ry, and we found that the remaining small discrepancies not visible on the figure can be further reduced by increasing the cutoff (see Fig. S2).

Zero point renormalization of energy levels at the DFT level of theory – We now turn to the discussion of electron-phonon self-energies. The real and imaginary parts of the electron-phonon self-energy yield the zero point renormalization and the lifetime of the single particle energy levels, respectively. To verify our implementation, we computed the ZPR of single particle energy levels in diamond at the DFT/LDA level of theory and compared our results with those reported in Ref. 3 and Ref. 11. In these two papers, the ZPRs are computed as

$$\Delta\varepsilon_{n\mathbf{k}}(T) = \frac{1}{N_{\mathbf{q}}} \sum_{\mathbf{q}\nu} \frac{\partial\varepsilon_{n\mathbf{k}}}{\partial n_{\mathbf{q}\nu}} \left[n_{\mathbf{q}\nu}(T) + \frac{1}{2} \right], \quad (18)$$

where $N_{\mathbf{q}}$ is the number of \mathbf{q} points and $\partial\varepsilon/\partial n$ is the electron-phonon coupling energy (EPCE). The latter can be evaluated using frozen-phonon or DFPT calculations,^{8,11} and

here we report our results using DFPT and the AHC approximation,^{11,22,23}

$$\frac{\partial \varepsilon_{n\mathbf{k}}^{FM}}{\partial n_{\nu\mathbf{q}}} = 2 \sum_m \frac{|g_{nm\nu}(\mathbf{k}, \mathbf{q})|^2}{\varepsilon_{n\mathbf{k}} - \varepsilon_{m\mathbf{k}+\mathbf{q}}}, \quad (19)$$

$$\frac{\partial \varepsilon_{n\mathbf{k}}^{DW}}{\partial n_{\nu\mathbf{q}}} = -\frac{1}{2\omega_{\mathbf{q}\nu}} \sum_m \sum_{I\alpha J\beta} \frac{1}{\varepsilon_{n\mathbf{k}} - \varepsilon_{m\mathbf{k}}} \left[\frac{\xi_{I\alpha, \mathbf{q}\nu} \xi_{I\beta, \mathbf{q}\nu}^*}{M_I} + \frac{\xi_{J\alpha, \mathbf{q}\nu} \xi_{J\beta, \mathbf{q}\nu}^*}{M_J} \right] g_{mn}^{*, I\alpha}(\mathbf{k}, \mathbf{0}) g_{mn}^{J\beta}(\mathbf{k}, \mathbf{0}). \quad (20)$$

We computed EPCEs with the Troullier-Martins type pseudopotential,²⁶ an energy cutoff of 60 Ry, and $6 \times 6 \times 6$ \mathbf{k} -point sampling, as in Ref. 11. We performed two sets of calculations, one using the lattice constant that we optimized at the LDA level (3.5185 Å), and the other using the lattice parameter (3.5323 Å) reported in Ref. 11. In Table 2 we compare the computed EPCEs with those in Ref. 11 at $\mathbf{k} = \Gamma$, L and $\mathbf{q} = \Gamma$, L . We find a mean absolute difference less than 3 meV and the mean absolute relative difference is $\sim 2\%$. The largest differences are observed at $(\mathbf{q} = \Gamma, \mathbf{k} = L_3)$ and $(\mathbf{q} = L, \mathbf{k} = \Gamma_{2'})$. For $(\mathbf{q} = \Gamma, \mathbf{k} = L_3)$, the EPCE computed with the optimized structure is -162.66 meV and the value reported in Ref. 11 is -180.55 meV; for $(\mathbf{q} = L, \mathbf{k} = \Gamma_{2'})$, the EPCE computed with our code and the lattice constant of Ref. 11 is -294.70 meV, to be compared to -307.54 meV, reported in Ref. 11.

Ref. 11 reported EPCEs' values but did not report renormalizations of energy levels in diamond. Therefore, to verify our computed renormalizations, we compare our results with those of Ref. 3, using the same lattice parameter (3.5473 Å) and $4 \times 4 \times 4$ \mathbf{k} -point sampling. The computed renormalization of the highest occupied and lowest unoccupied bands at the Γ point are 116 and -319 meV, respectively, in good agreement with the values of 113 and -314 meV, reported in Ref. 3. As a result, our computed renormalization of the direct gap in diamond is -439 meV, which also agrees very well with the result -427 meV of Ref. 3.

We also evaluated the Fan-Migdal self-energy without adopting the AHC approximation and thus considering so called non-adiabatic terms, by including phonon frequencies in the denominator of Eq. 13. We emphasize that in our approach, which does not re-

Table 2: Electron-phonon coupling energies (see Eq. 18) [meV] computed with optimized cell parameters (third column) and with the cell parameters reported by Ref. 11 (fourth column). Mean absolute differences (MAD)[meV] and mean absolute relative differences (MARD) are given in the last row.

q point	k point	Optimized Cell	Cell parameter from Ref. 11	Ref. 11
Γ	Γ_1	-12.55	-12.84	-12.53
	$\Gamma_{25'}$	25.13	24.86	24.83
	Γ_{15}	-14.87	-14.88	-14.23
	$\Gamma_{2'}$	-31.91	-30.86	-30.93
	$L_{2'}$	-21.18	-21.54	-20.98
	L_1	-16.72	-16.91	-16.60
	$L_{3'}$	10.14	10.02	10.10
	L_3	-162.66	-182.88	-180.55
L	Γ_1	-54.47	-55.15	-53.73
	$\Gamma_{25'}$	186.17	186.71	181.28
	Γ_{15}	-273.16	-274.86	-273.58
	$\Gamma_{2'}$	-311.89	-294.70	-307.54
	$L_{2'}$	-91.27	-91.96	-89.36
	L_1	-212.64	-224.15	-220.56
	$L_{3'}$	-26.88	-27.13	-25.91
	L_3	163.96	164.07	163.19
MAD [meV]		2.63	2.10	
MARD [%]		2.29 %	2.13 %	

quire summations over empty bands, the inclusion of non-adiabatic effects comes at no extra computational cost, as does the evaluation of electron-phonon self energies at multiple temperatures and frequencies. We found that the ZPR of the indirect band gap of diamond computed by including non-adiabatic effects is -332 meV, in good agreement with the value -327 meV reported in Ref. 11, where the LDA functional and $10 \times 10 \times 10$ \mathbf{k} -point sampling were used, as in our work.

We close the discussion of our DFT results by presenting temperature-dependent renormalizations of both the direct and indirect gaps in diamond obtained with $4 \times 4 \times 4$ \mathbf{q} -point sampling (Fig. 1). We carried out the calculations with the LDA functional at the LDA lattice constant obtained in Ref. 3, and with the PBE functional and the optimized lattice constant at the PBE level of theory. We find an almost identical temperature dependence with the two functionals. Our results for the direct gap renormalization compare well with those of Ref. 15 and 28; however, they differ from those of Ref. 3. As for the indirect gap, our results agree well with those obtained from frozen-phonon calculations¹⁴ and with the findings of Ref. 28 for temperatures lower than 500 K, however we find larger differences at higher temperature.

Zero point renormalization of energy levels at the G_0W_0 level of theory – We conducted a detailed study of the zero point renormalization of the direct gap of diamond at the level of G_0W_0 , using different numerical protocols, denoted P1 – P5 in Table 3. Our fully-converged result is -545 meV (P1 in Table 3), which is smaller than the value reported in Ref. 3. We investigated the dependence of the results on N_{states} , the number of states used in the evaluation of the G_0W_0 self-energy; on whether the Lanczos approach was used in the evaluation of G_0W_0 and electron-phonon self-energies; and on whether a full-frequency (FF) integration or the Hybersten-Louie plasmon-pole model (PPM) was used in the evaluation of the G_0W_0 self-energy. The G_0W_0 calculation with the PPM was carried out with the ABINIT package.^{31,32} In addition, we used the curvature technique proposed in Ref. 33 in the calculation of the exchange part of the G_0W_0 self-energy.

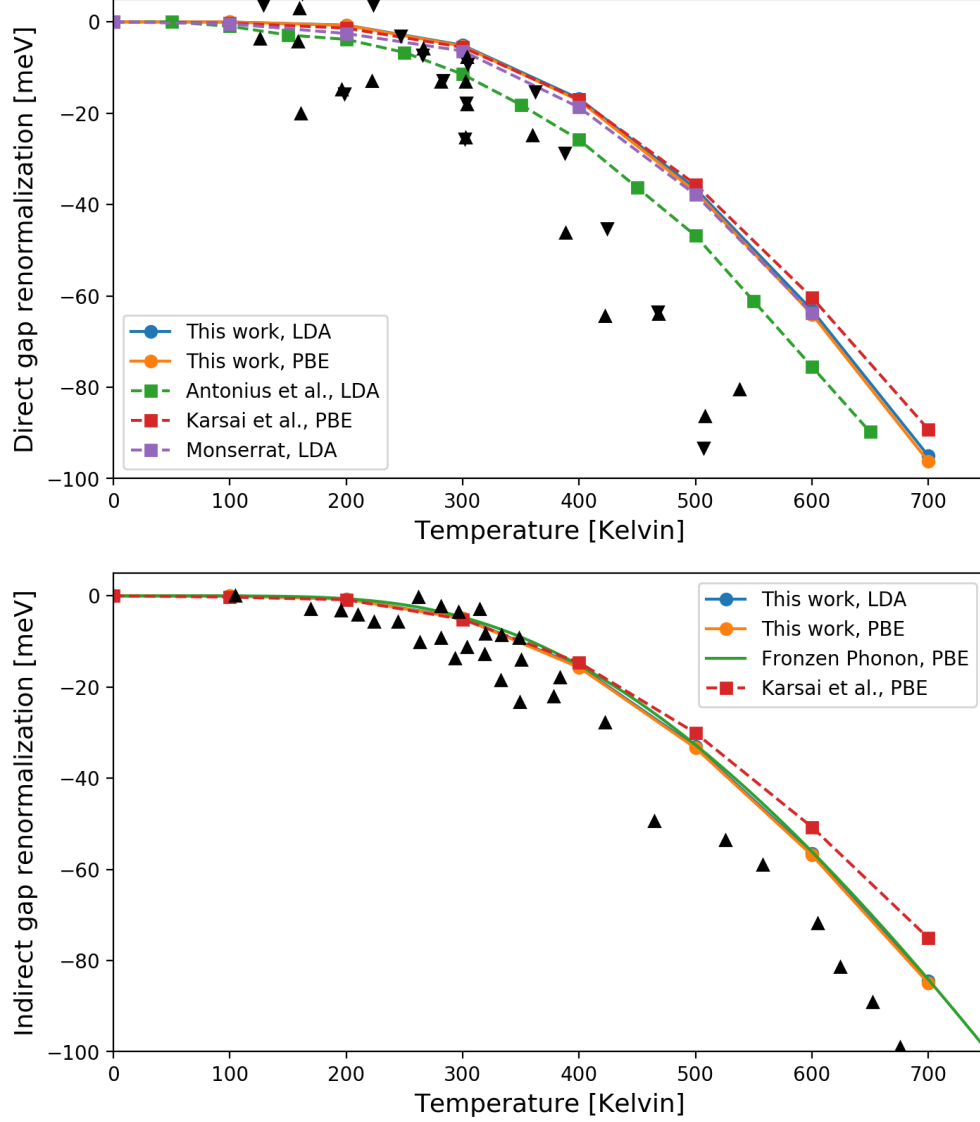


Figure 1: Temperature dependence of direct (upper) and indirect (lower) band gap in diamond. The renormalization at zero temperature was set at zero. The literature calculations are Antonius et al. (Ref. 3), Karsai et al. (Ref. 28) and Monserrat (Ref. 15), and the experimental renormalizations (black triangles) of direct and indirect gap are extracted from Ref. 29 and Ref. 30, respectively.

In Table 3, P1 and P2 both yield what we consider a converged value of the ZPR -545 meV, obtained by using 8 bands (4 valence bands and 4 conduction bands) and 100 bands (4 valence bands and 96 conduction bands), respectively. In P3, the curvature correction was not adopted when computing the exchange part of the electron self-energies and the computed ZPR, -562 meV, was about 20 meV lower than our converged value. In P4, where the Lanczos approach was not adopted, we obtained an even lower value, -600 meV. For P1 – P4, the G_0W_0 quasiparticle energies were obtained with the **WEST** code²⁰ with full-frequency (FF) integration. Finally in P5 we used the G_0W_0 band structure obtained with the plasmon-pole model (PPM) computed with the **ABINIT** package, as input for our calculations. By doing so we obtain a ZPR of -620 meV, in good agreement with the result -622 meV reported in Ref. 3.

This comparison shows that the accuracy of G_0W_0 corrections to DFT eigenvalues has a significant impact on the computed electron-phonon self-energies; the comparison also shows that the plasmon-pole model may not be sufficiently accurate even for a simple crystal such as diamond.

Table 3: Zero point renormalization (ZPR) of the direct gap of diamond obtained with different computational protocols (P) at the level of G_0W_0 @LDA. N_{states} denotes the number of empty bands used in the evaluation of the G_0W_0 self-energy; Lanczos the algorithm used for the frequency integration; FF and PPM stand for full frequency and plasmon pole model, respectively. In the last row we indicate whether the curvature technique of Ref. 33 was included in the calculation of the exact exchange term of the self-energy.

	P1	P2	P3	P4	P5	Ref. 3
ZPR [meV]	-545	-545	-562	-600	-620	-622
$N_{\text{states}} (\Sigma_{G_0W_0})$	8	100	100	100	100	100
Lanczos ($\Sigma_{G_0W_0}$)	Yes	Yes	Yes	No	No	No
Lanczos (Σ_{ep})	Yes	Yes	Yes	Yes	Yes	See text
Freq. integration	FF	FF	FF	FF	PPM	PPM
Curvature	Yes	Yes	No	No	No	N/A

Large scale calculations: zero point renormalization in defective solids

After verifying our implementation and examining the effect of various numerical approximations, we carried out calculations for supercells representative of defective solids, in particular defects in diamond (see Figure 2), showcasing the ability of the methodology developed here to carry out calculations for large systems. We considered two nearest neighbor carbon atoms replaced by either two boron or two nitrogen atoms. The electronic structure of the boron (nitrogen) pair exhibits one unoccupied (occupied) state in the band gap of the host. We carried out DFT calculations with the PBE functional,³⁴ SG15³⁵ ONCV³⁶ pseudopotentials and an energy cutoff of 50 Ry. The G_0W_0 calculations were carried out with the WEST code. We report the electron-phonon renormalizations of the systems with defects in Table 4 and Table 5.

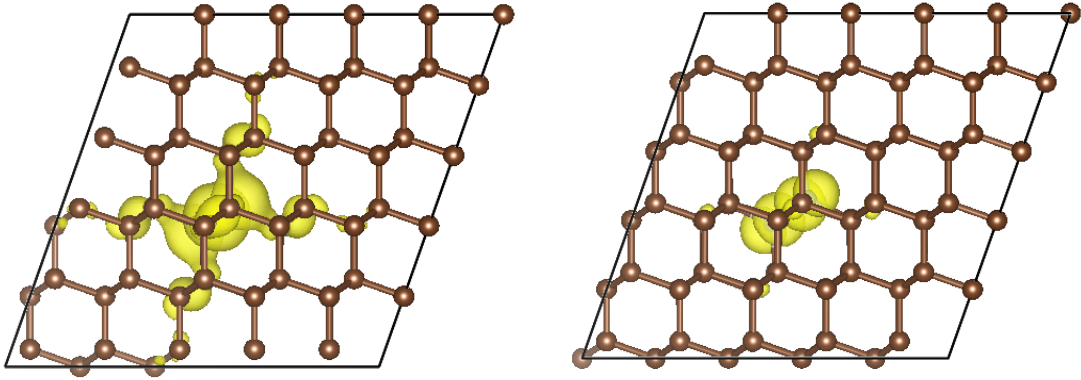


Figure 2: Isosurface (yellow) of the square moduli of the single particle orbitals of the boron pair unoccupied defect state (left) and nitrogen pair occupied defect state (right), as obtained in a $5 \times 5 \times 5$ supercell of diamond.

We first discuss the results using the AHC approximation (Table 4 and Table 5). The presence of defects affects the renormalization of the gap of the host crystal due to symmetry breaking,¹⁴ with the effect decreasing in magnitude as the size of supercell increases, as expected. In order to find a converged value of the renormalization, we extrapolated our computed values as a function of the inverse of the supercell size for defective systems, and

as a function of the inverse of the number of \mathbf{q} -points for pristine diamond. Our extrapolated values at the PBE level are -340 meV for the gap of pristine diamond and -338 and -370 meV for that of diamond with boron and nitrogen pairs, respectively. Once we add G_0W_0 corrections, the corresponding extrapolated values are -351 meV and -372 and -386 meV. In all cases, within the AHC approximations, we do not find significant differences between the renormalizations of the gap of pristine and defective diamond.

The renormalization of the defect state within the band gap is more interesting, as the renormalizations of the defect states arising from boron and nitrogen pairs are noticeably distinct, 51 meV and -7 meV, respectively, at the PBE level, after extrapolation. When adding G_0W_0 corrections, the extrapolated values are 40 meV and 1 meV.

We now turn to discuss non-adiabatic effects. We found that including non-adiabatic effects in Eq. 13 changes substantially the renormalizations computed for defect states in diamond, although it has a smaller effect on the gap of diamond. Our results are reported in Table 4 and Table 5. The gap of diamond varies by -56 , -35 and -12 meV when including non-adiabatic effect, in the case of the pristine solid, boron and nitrogen defective systems, respectively, at the PBE level in the $5 \times 5 \times 5$ supercell. The magnitude of the renormalization of defect states increases by approximately a factor of 3 for boron pairs and by more than a factor of 10 for nitrogen in $5 \times 5 \times 5$ supercell, when including non-adiabatic effects. After extrapolation, the renormalization of the boron defect state is -86 meV(PBE) and -99 meV(G_0W_0) and that of the nitrogen pair is 138 meV(PBE) and 141 meV (G_0W_0).

To understand the difference between the results obtained with and without non-adiabatic effects, we plot in Figure 3 the contribution of each vibrational mode to the difference between the adiabatic and non-adiabatic renormalizations for the boron pair, described with a $5 \times 5 \times 5$ supercell; such difference is expressed in terms of the fractional contribution of defect atoms to each mode, $f_{\mathbf{q}\nu}^{\text{defect}} = \sum_I^{\text{defect}} \sum_{\alpha} |\xi_{I\alpha, \mathbf{q}\nu}|^2$, where the summation runs over the boron atoms. We define vibrational modes with $f_{\mathbf{q}\nu}^{\text{defect}} > 10\%$ as modes exhibiting defect relevant vibrations. Figure 3 shows that defect relevant vibrations are indeed responsible

Table 4: Zero point renormalization (ZPR) [meV] of pristine diamond (last column) and of diamond hosting defects (Host), and of defect states (Defect).

	Supercell	ZPR (Defect)	ZPR (Host)	ZPR (Pristine)
Adiabatic DFT/PBE	$3 \times 3 \times 3$	36	-397	-277
	$4 \times 4 \times 4$	46	-401	-366
	$5 \times 5 \times 5$	47	-327	-316
	$6 \times 6 \times 6$	—	—	-324
	$8 \times 8 \times 8$	—	—	-330
	$10 \times 10 \times 10$	—	—	-341
	extrapolated	51 ^a	-338 ^a	-357 ^a , -340 ^b
Adiabatic G_0W_0 @PBE	$3 \times 3 \times 3$	29	-416	-254
	$4 \times 4 \times 4$	37	-448	-380
	$5 \times 5 \times 5$	37	-346	-291
	extrapolated	40 ^a	-372 ^a	-351 ^a
Non-adiabatic DFT/PBE	$3 \times 3 \times 3$	-267	-556	-637
	$4 \times 4 \times 4$	-152	-482	-510
	$5 \times 5 \times 5$	-131	-362	-372
	$6 \times 6 \times 6$	—	—	-353
	$8 \times 8 \times 8$	—	—	-330
	$10 \times 10 \times 10$	—	—	-329
	extrapolated	-86 ^a	-346 ^a	-338 ^a , -320 ^b
Non-adiabatic G_0W_0 @PBE	$3 \times 3 \times 3$	-275	-574	-615
	$4 \times 4 \times 4$	-163	-518	-508
	$5 \times 5 \times 5$	-143	-379	-348
	extrapolated	-99 ^a	-373 ^a	-325 ^a

^a Extrapolated up to $5 \times 5 \times 5$

^b Extrapolated up to $10 \times 10 \times 10$

Table 5: Zero point renormalization (ZPR) [meV] of pristine diamond (last column) and of diamond hosting defects (Host), and of defect states (Defect).

	Supercell	ZPR (Defect)	ZPR (Host)	ZPR (Pristine)
Adiabatic DFT/PBE	$3 \times 3 \times 3$	22	-322	-277
	$4 \times 4 \times 4$	3	-394	-366
	$5 \times 5 \times 5$	1	-333	-316
	$6 \times 6 \times 6$	—	—	-324
	$8 \times 8 \times 8$	—	—	-330
	$10 \times 10 \times 10$	—	—	-341
	extrapolated	-7 ^a	-370 ^a	-357 ^a , -340 ^b
Adiabatic G_0W_0 @PBE	$3 \times 3 \times 3$	33	-339	-254
	$4 \times 4 \times 4$	12	-415	-380
	$5 \times 5 \times 5$	9	-346	-291
	extrapolated	1 ^a	-386 ^a	-351 ^a
Non-adiabatic DFT/PBE	$3 \times 3 \times 3$	185	-459	-637
	$4 \times 4 \times 4$	156	-431	-510
	$5 \times 5 \times 5$	149	-345	-372
	$6 \times 6 \times 6$	—	—	-353
	$8 \times 8 \times 8$	—	—	-330
	$10 \times 10 \times 10$	—	—	-329
	extrapolated	138 ^a	-344 ^a	-338 ^a , -320 ^b
Non-adiabatic G_0W_0 @PBE	$3 \times 3 \times 3$	192	-473	-615
	$4 \times 4 \times 4$	161	-452	-508
	$5 \times 5 \times 5$	153	-359	-348
	extrapolated	141 ^a	-362 ^a	-325 ^a

^a Extrapolated up to $5 \times 5 \times 5$

^b Extrapolated up to $10 \times 10 \times 10$

for the difference between adiabatic and non-adiabatic effects found in the case of defect states; however their contribution to the host gap renormalization are small. Quantitatively, the defect relevant vibrations contribute approximately -89 meV to the difference between adiabatic and non-adiabatic defect state renormalizations, with the remaining -88 meV being accounted for by coupling with lattice vibrations. Overall our results indicate that the AHC formalism and related adiabatic approximation are not sufficiently accurate to describe the electron-phonon renormalizations of carbon-based defect states, and that taking into account non-adiabatic effects is critical to obtain accurate results.

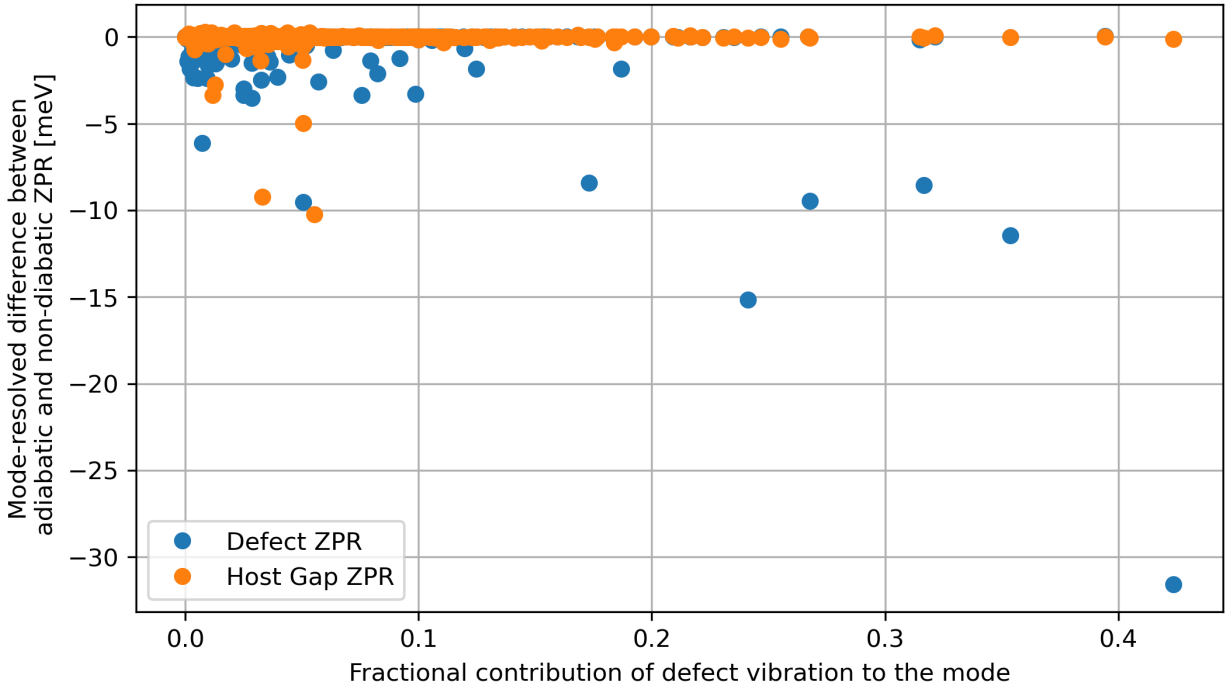


Figure 3: The contribution of vibration modes to the difference between adiabatic and non-adiabatic renormalizations for a boron pair in diamond, described in a $5 \times 5 \times 5$ supercell, with respect to the fractional contribution of the vibration of defect atoms $f_{\mathbf{q}\nu}^{\text{defect}}$ (see text).

Conclusion

In summary, we presented an efficient, combined approach to compute electron-electron and electron-phonon self-energies in solids, which can be used for large scale calculations, and

enables the inclusion of non-adiabatic and temperature effects in a simple, straightforward manner, at no extra computational cost. This approach is a generalization to solid of the method proposed for molecules in Ref. 17. We discussed in detail verification and validation strategies for calculations at the DFT and G_0W_0 level of theory; we found that the numerical accuracy of G_0W_0 band structures is critical to obtain robust predictions of zero point renormalizations of energy levels and that carrying out full frequency integration is necessary to reach the required accuracy. We presented calculations for pristine diamond and defects in diamonds with supercells containing ~ 1000 electrons; we found that while the inclusion of non-adiabatic effects leads to moderate changes in the renormalization of the diamond band gap, it is essential to obtain accurate results for defect levels in the gap. Work is in progress to apply our methodology to the study of spin-defects in diamond and in other insulators and semiconductors, including spin-phonon interaction.

Acknowledgement

We thank He Ma and Ryan L. McAvoy for useful discussion. This work was supported by the Midwest Integrated Center for Computational Materials (MICCoM) as part of the Computational Materials Sciences Program funded by the U.S. Department of Energy. This research used resources of the National Energy Research Scientific Computing Center (NERSC), a DOE Office of Science User Facility supported by the Office of Science of the U.S. Department of Energy under Contract No. DE-AC02-05CH11231, resources of the Argonne Leadership Computing Facility, which is a DOE Office of Science User Facility supported under Contract DE-AC02-06CH11357, and resources of the University of Chicago Research Computing Center.

References

- (1) Giustino, F. Electron-phonon interactions from first principles. *Reviews of Modern Physics* **2017**, *89*, 015003.
- (2) Giustino, F.; Louie, S. G.; Cohen, M. L. Electron-phonon renormalization of the direct band gap of diamond. *Physical review letters* **2010**, *105*, 265501.
- (3) Antonius, G.; Poncé, S.; Boulanger, P.; Côté, M.; Gonze, X. Many-body effects on the zero-point renormalization of the band structure. *Physical Review Letters* **2014**, *112*, 215501.
- (4) Bardeen, J.; Cooper, L. N.; Schrieffer, J. R. Microscopic theory of superconductivity. *Physical Review* **1957**, *106*, 162.
- (5) Fan, H. Temperature dependence of the energy gap in semiconductors. *Physical Review* **1951**, *82*, 900.
- (6) Fröhlich, H.; Pelzer, H.; Zienau, S. XX. Properties of slow electrons in polar materials. *The London, Edinburgh, and Dublin Philosophical Magazine and Journal of Science* **1950**, *41*, 221–242.
- (7) Giustino, F.; Cohen, M. L.; Louie, S. G. Electron-phonon interaction using Wannier functions. *Physical Review B* **2007**, *76*, 165108.
- (8) Monserrat, B. Electron–phonon coupling from finite differences. *Journal of Physics: Condensed Matter* **2018**, *30*, 083001.
- (9) Giannozzi, P.; De Gironcoli, S.; Pavone, P.; Baroni, S. Ab initio calculation of phonon dispersions in semiconductors. *Physical Review B* **1991**, *43*, 7231.
- (10) Baroni, S.; De Gironcoli, S.; Dal Corso, A.; Giannozzi, P. Phonons and related crystal properties from density-functional perturbation theory. *Reviews of Modern Physics* **2001**, *73*, 515.

- (11) Poncé, S.; Antonius, G.; Gillet, Y.; Boulanger, P.; Janssen, J. L.; Marini, A.; Côté, M.; Gonze, X. Temperature dependence of electronic eigenenergies in the adiabatic harmonic approximation. *Physical Review B* **2014**, *90*, 214304.
- (12) Cannuccia, E.; Marini, A. Effect of the quantum zero-point atomic motion on the optical and electronic properties of diamond and trans-polyacetylene. *Physical review letters* **2011**, *107*, 255501.
- (13) Cannuccia, E.; Marini, A. Zero point motion effect on the electronic properties of diamond, trans-polyacetylene and polyethylene. *The European Physical Journal B* **2012**, *85*, 320.
- (14) Kundu, A.; Govoni, M.; Yang, H.; Ceriotti, M.; Gygi, F.; Galli, G. Quantum vibronic effects on the electronic properties of solid and molecular carbon. 2021.
- (15) Monserrat, B. Correlation effects on electron-phonon coupling in semiconductors: Many-body theory along thermal lines. *Physical Review B* **2016**, *93*, 100301.
- (16) Martin, R. M.; Reining, L.; Ceperley, D. M. *Interacting electrons*; Cambridge University Press, 2016.
- (17) McAvoy, R. L.; Govoni, M.; Galli, G. Coupling First-Principles Calculations of Electron–Electron and Electron–Phonon Scattering, and Applications to Carbon-Based Nanostructures. *Journal of chemical theory and computation* **2018**, *14*, 6269–6275.
- (18) Wilson, H. F.; Lu, D.; Gygi, F.; Galli, G. Iterative calculations of dielectric eigenvalue spectra. *Physical Review B* **2009**, *79*, 245106.
- (19) Pham, T. A.; Nguyen, H.-V.; Rocca, D.; Galli, G. G W calculations using the spectral decomposition of the dielectric matrix: Verification, validation, and comparison of methods. *Physical Review B* **2013**, *87*, 155148.

- (20) Govoni, M.; Galli, G. Large scale GW calculations. *Journal of chemical theory and computation* **2015**, *11*, 2680–2696.
- (21) Govoni, M.; Galli, G. GW100: comparison of methods and accuracy of results obtained with the WEST code. *Journal of chemical theory and computation* **2018**, *14*, 1895–1909.
- (22) Allen, P. B.; Heine, V. Theory of the temperature dependence of electronic band structures. *Journal of Physics C: Solid State Physics* **1976**, *9*, 2305.
- (23) Allen, P.; Cardona, M. Theory of the temperature dependence of the direct gap of germanium. *Physical Review B* **1981**, *23*, 1495.
- (24) Giannozzi, P.; Baroni, S.; Bonini, N.; Calandra, M.; Car, R.; Cavazzoni, C.; Ceresoli, D.; Chiarotti, G. L.; Cococcioni, M.; Dabo, I., et al. QUANTUM ESPRESSO: a modular and open-source software project for quantum simulations of materials. *Journal of physics: Condensed matter* **2009**, *21*, 395502.
- (25) Godby, R. W.; Schlüter, M.; Sham, L. Self-energy operators and exchange-correlation potentials in semiconductors. *Physical Review B* **1988**, *37*, 10159.
- (26) Troullier, N.; Martins, J. L. Efficient pseudopotentials for plane-wave calculations. *Physical review B* **1991**, *43*, 1993.
- (27) Fuchs, M.; Scheffler, M. Ab initio pseudopotentials for electronic structure calculations of poly-atomic systems using density-functional theory. *Computer Physics Communications* **1999**, *119*, 67–98.
- (28) Karsai, F.; Engel, M.; Flage-Larsen, E.; Kresse, G. Electron–phonon coupling in semiconductors within the GW approximation. *New Journal of Physics* **2018**, *20*, 123008.
- (29) Logothetidis, S.; Petalas, J.; Polatoglou, H.; Fuchs, D. Origin and temperature dependence of the first direct gap of diamond. *Physical Review B* **1992**, *46*, 4483.

- (30) O’donnell, K.; Chen, X. Temperature dependence of semiconductor band gaps. *Applied physics letters* **1991**, *58*, 2924–2926.
- (31) Gonze, X.; Amadon, B.; Antonius, G.; Arnardi, F.; Baguet, L.; Beuken, J.-M.; Bieder, J.; Bottin, F.; Bouchet, J.; Bousquet, E., et al. The ABINIT project: Impact, environment and recent developments. *Computer Physics Communications* **2020**, *248*, 107042.
- (32) Bruneval, F.; Vast, N.; Reining, L. Effect of self-consistency on quasiparticles in solids. *Physical Review B* **2006**, *74*, 045102.
- (33) Nguyen, H.-V.; de Gironcoli, S. Efficient calculation of exact exchange and RPA correlation energies in the adiabatic-connection fluctuation-dissipation theory. *Physical Review B* **2009**, *79*, 205114.
- (34) Perdew, J. P.; Burke, K.; Ernzerhof, M. Generalized gradient approximation made simple. *Physical review letters* **1996**, *77*, 3865.
- (35) Schlipf, M.; Gygi, F. Optimization algorithm for the generation of ONCV pseudopotentials. *Computer Physics Communications* **2015**, *196*, 36–44.
- (36) Hamann, D. Optimized norm-conserving Vanderbilt pseudopotentials. *Physical Review B* **2013**, *88*, 085117.

Supplementary Information: Combined first-principles calculations of electron-electron and electron-phonon self-energies in condensed systems

Han Yang,^{†,‡} Marco Govoni,^{*,¶,‡} Arpan Kundu,[‡] and Giulia Galli^{*,†,‡,¶}

[†]*Department of Chemistry, University of Chicago, Chicago, Illinois 60637, United States*

[‡]*Pritzker School of Molecular Engineering, The University of Chicago, Chicago, Illinois 60637, United States*

[¶]*Materials Science Division and Center for Molecular Engineering, Argonne National Laboratory, Lemont, Illinois 60439, United States*

E-mail: mgovoni@anl.gov; gagalli@uchicago.edu

Evaluation of electron-phonon self-energies with the Lanczos approach

We discuss an approach based on the Lanczos method,¹ to avoid summation over empty bands when computing the electron-phonon self-energy. Starting from Eq. 17 of the main text, we define $A_{n\mathbf{k}}(\tilde{H}_{\mathbf{k}+\mathbf{q}}) = (\varepsilon_{n\mathbf{k}} - \tilde{H}_{\mathbf{k}+\mathbf{q}})^{-1}$, and Eq. 17 can be written as,

$$A_{n\mathbf{k}}(\tilde{H}_{\mathbf{k}+\mathbf{q}}) = \sum_m |\psi_{m\mathbf{k}+\mathbf{q}}\rangle A_{n\mathbf{k}}(\varepsilon_{m\mathbf{k}+\mathbf{q}}) \langle\psi_{m\mathbf{k}+\mathbf{q}}| \quad (1)$$

Following references,^{1,2} we obtain the Lanczos basis \tilde{q}_l and corresponding eigenvalues d_l of $\tilde{H}_{\mathbf{k}+\mathbf{q}}$, and thus the self-energy can be written as

$$\Sigma_{n\mathbf{k}}^{FM}(T) = \sum_{\nu\mathbf{q}l} \langle L_{n\mathbf{k}}^{\mathbf{q}\nu} | \tilde{q}_l \rangle A_{n\mathbf{k}}(d_l) \langle \tilde{q}_l | R_{n\mathbf{k}}^{\mathbf{q}\nu} \rangle [2n_{\mathbf{q}\nu}(T) + 1], \quad (2)$$

where $|L_{n\mathbf{k}}^{\mathbf{q}\nu}\rangle$ and $|R_{n\mathbf{k}}^{\mathbf{q}\nu}\rangle$ are vectors within the set $\{|\partial_{\mathbf{q}\nu} V_{SCF} \psi_{n\mathbf{k}}\rangle, n = 1, 2, \dots\}$.

In the following, we describe how to compute Lanczos basis functions, and hereafter we drop the superscripts and subscripts of $|L\rangle$ and $|R\rangle$ for simplicity. The Lanczos basis functions and eigenvalues can be obtained by diagonalizing the matrix

$$Q^\dagger \tilde{H} Q = \begin{pmatrix} \alpha_1 & \beta_2 & & & \\ \beta_2 & \alpha_2 & \beta_3 & & \\ & \beta_3 & \ddots & \ddots & \\ & & \ddots & \ddots & \beta_n \\ & & & \beta_n & \alpha_n \end{pmatrix} \quad (3)$$

where $Q = \{|q_l\rangle, l = 1, 2, \dots, N_{\text{Lanczos}}\}$ with $|q_1\rangle = |R\rangle$ are a set of orthonormal vectors, and the elements of the matrix are obtained from

$$\alpha_n = \langle q_l | \tilde{H} | q_l \rangle \quad (4)$$

and

$$\beta_{n+1} = \|(\tilde{H} - \alpha_n) |q_n\rangle - \beta_n |q_{n-1}\rangle\|. \quad (5)$$

The vectors $|q_l\rangle$ are orthogonalized with a recursive process by applying

$$|q_{n+1}\rangle = \frac{1}{\beta_{n+1}} \left[(\tilde{H} - \alpha_n) |q_n\rangle - \beta_n |q_{n-1}\rangle \right]. \quad (6)$$

The diagonalization of Eq. 3 yields the eigenvalues d_l and corresponding eigenvectors U_l . We

then define a modified basis set $|\tilde{q}_l\rangle$ as a linear combination of the original basis $|q_l\rangle$,

$$|\tilde{q}_l\rangle = \sum_k^{N_{\text{Lanczos}}} U_l^k |q_k\rangle. \quad (7)$$

Having obtained the eigenvalues d_l of the matrix $Q^\dagger \tilde{H} Q$ and using the modified basis $|\tilde{q}_l\rangle$, we can evaluate the Fan-Migdal self-energy in Eq. 2, without summations over empty bands. A similar technique can be applied to obtain the Debye-Waller self-energy.

In addition, we can compute the temperature-dependent, non-adiabatic or frequency-dependent self-energies without any extra computational cost, by reusing the Lanczos basis set defined above.

Convergence study of phonon frequencies in diamond

To verify our implementation, we computed phonon frequencies with the method described in the main text with the LDA functional and 60 Ry cutoff, and compared them with the results obtained with the PHonon³ code. Fig. 1 shows the phonon dispersion curves computed with our code and the PHonon code, which are indistinguishable.

We also carried out additional comparisons with higher energy cutoffs and in Fig. 2 we report the differences of the phonon frequencies with different energy cutoffs. As the energy cutoff increases, both methods converge to the same phonon frequencies.

Pseudopotentials used in this paper

In Table 1, we list the pseudopotentials that were used in this work.

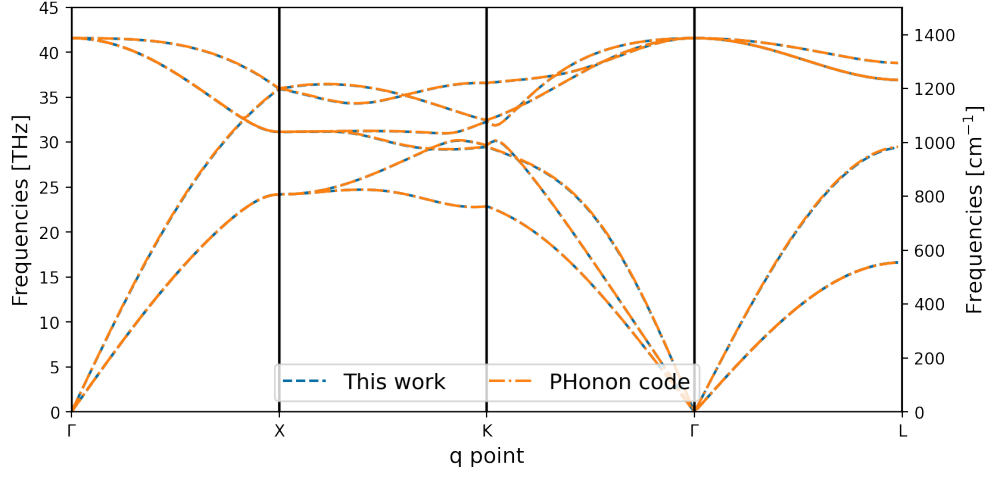


Figure 1: Phonon dispersion of diamond interpolated from $3 \times 3 \times 3$ \mathbf{q} -point sampling. A kinetic energy cutoff of 60 Ry and LDA functional were used.

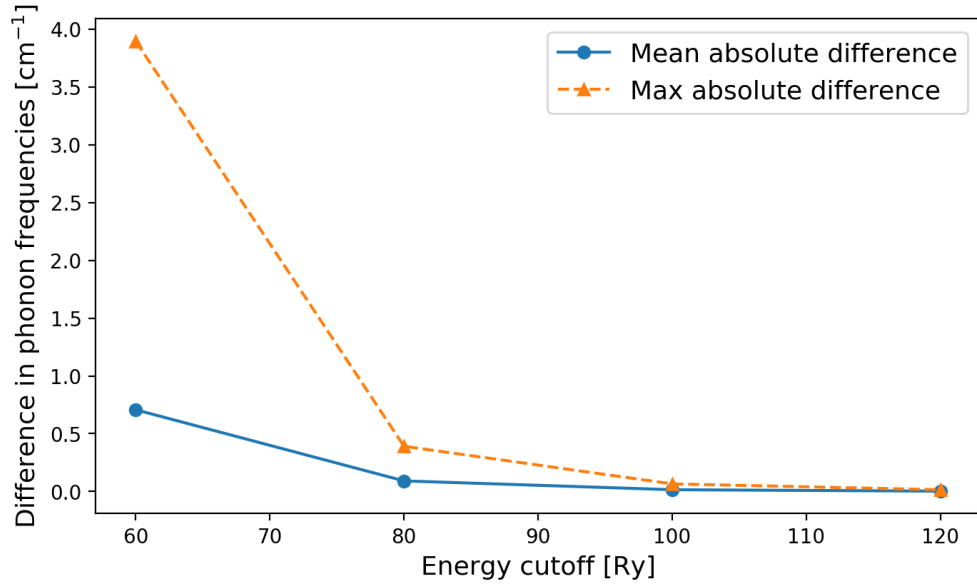


Figure 2: Mean and maximum absolute difference of phonon frequencies [in cm^{-1}] computed with the method discussed in this work and the PHonon package in Quantum Espresso.

Table 1: Pseudopotentials used in this paper

Pseudopotential	Comment
C.pz-mt.fhi.UPF	Martins-Troullier ⁴ type pseudopotential of carbon generated with Perdew-Zunger ⁵ parameterized LDA functional in UPF format and is ready for Quantum Espresso calculation.
C.pz-mt.fhi	Martins-Troullier ⁴ type pseudopotential of carbon generated with Perdew-Zunger ⁵ parameterized LDA functional in fhi format and is ready for ABINIT calculation.
C_ONCV_PBE-1.0.upf	SG15 ⁶ ONCV ⁷ pseudopotential of carbon generated with PBE functional ⁸ and is ready for Quantum Espresso calculation.
B_ONCV_PBE-1.0.upf	SG15 ⁶ ONCV ⁷ pseudopotential of boron generated with PBE functional ⁸ and is ready for Quantum Espresso calculation.
N_ONCV_PBE-1.0.upf	SG15 ⁶ ONCV ⁷ pseudopotential of nitrogen generated with PBE functional ⁸ and is ready for Quantum Espresso calculation.

References

- (1) Lanczos, C. An iteration method for the solution of the eigenvalue problem of linear differential and integral operators. **1950**,
- (2) McAvoy, R. L.; Govoni, M.; Galli, G. Coupling First-Principles Calculations of Electron–Electron and Electron–Phonon Scattering, and Applications to Carbon-Based Nanostructures. *Journal of chemical theory and computation* **2018**, *14*, 6269–6275.
- (3) Giannozzi, P.; Baroni, S.; Bonini, N.; Calandra, M.; Car, R.; Cavazzoni, C.; Ceresoli, D.; Chiarotti, G. L.; Cococcioni, M.; Dabo, I., et al. QUANTUM ESPRESSO: a modular and open-source software project for quantum simulations of materials. *Journal of physics: Condensed matter* **2009**, *21*, 395502.
- (4) Troullier, N.; Martins, J. L. Efficient pseudopotentials for plane-wave calculations. *Physical review B* **1991**, *43*, 1993.
- (5) Perdew, J. P.; Zunger, A. Self-interaction correction to density-functional approximations for many-electron systems. *Physical Review B* **1981**, *23*, 5048.
- (6) Schlipf, M.; Gygi, F. Optimization algorithm for the generation of ONCV pseudopotentials. *Computer Physics Communications* **2015**, *196*, 36–44.
- (7) Hamann, D. Optimized norm-conserving Vanderbilt pseudopotentials. *Physical Review B* **2013**, *88*, 085117.
- (8) Perdew, J. P.; Burke, K.; Ernzerhof, M. Generalized gradient approximation made simple. *Physical review letters* **1996**, *77*, 3865.